Geophysical Research Letters

RESEARCH LETTER
10.1029/2018GL080594

Tsunami versus Infragravity Surge: Comparison of the Physical Character of Extreme Runup

Luis Montoya[1] and **Patrick Lynett**[1]

[1]Tsunami Research Center, Sonny Astani Department of Civil and Environmental Engineering, University of Southern California, Los Angeles, CA, USA

Abstract Recent observations of energetic infragravity (IG) flooding events, such as those in the Philippines during Typhoon Haiyan, suggest that IG surges may approach the coast as breaking bores with periods of minutes: a very tsunami-like characteristic. Energetic IG waves have been observed in various locations around the world and have led to loss of lives and damages to property. In this study, a comparison of overland flow characteristics between tsunamis and energetic IG wave events is presented. In general, whenever the tsunamis and energetic IG waves have similar runup, tsunamis tend to generate greater flow depths and longer flood durations than IG. However, flow velocities and Froude number are larger for IG primarily due to bore-bore capture. This study provides a statistical and physical discriminant between tsunami and IG, such that in areas exposed to both, a proper interpretation of overland transport, deposition, and damage is possible.

Plain Language Summary Traditionally, discoveries of sediment layers that are located far away from the shoreline (>150 m) are usually attributed to tsunami events because it is assumed that wind waves cannot reach those limits. But, recent observations of energetic infragravity waves (lower frequency than ordinary waves), such as those in the Philippines during Typhoon Haiyan, have led to an increase in awareness of such events. Infragravity flooding events, also known as sneaker waves, tend to appear very *tsunami-like*; due to the long distance the wave travels inland, inundating the coast. In this study, numerical simulations were used to estimate flood duration, flow depths, and speeds from potential energetic infragravity waves, and these were compared with similar values from tsunamis. Our analysis shows that tsunamis tend to flood the beach for a longer time than infragavity waves. Also, flow depths from tsunamis were larger. Contrarily, infragravity waves were found to have greater velocities than tsunamis. The purpose of this study is to better understand the flow properties of tsunami and infragravity, so that a proper interpretation of overland transport, sediment accumulation, and damage can be achieved in the areas exposed to both events.

Key Points:
- Extreme infragravity-driven runup events can lead to runup elevations comparable to those of tsunamis
- Comparisons of flood duration, flow depth, flow speeds, and Froude number between infragravity and tsunami are presented
- In general, tsunami inundation generated greater flood duration and flow depths, while infragravity yielded greater flow speeds and Froude numbers

Supporting Information:
- Supporting Information S1

Correspondence to:
L. Montoya,
lhmontoy@usc.edu

Citation:
Montoya, L., & Lynett, P. (2018). Tsunami versus infragravity surge: Comparison of the physical character of extreme runup. *Geophysical Research Letters*, *45*, 12,982–12,990. https://doi.org/10.1029/2018GL080594

Received 22 SEP 2018
Accepted 20 NOV 2018
Accepted article online 28 NOV 2018
Published online 12 DEC 2018
Corrected 24 JAN 2019

This article was corrected on 24 JAN 2019. See the end of the full text for details.

1. Introduction

Sediment deposits that are discovered somewhat far-away from the shoreline (>150 m) are usually attributed to past tsunami events (e.g., Morton et al., 2007; Phantuwongraj & Choowong, 2012). Generally, scientists assume that wind wave-driven runup cannot reach those limits (e.g., Cox et al., 2018). Furthermore, geologists characterize deposits based on the hydrodynamic differences between tsunamis and storm, which create distinctive sedimentary patterns (Mamo et al., 2009; Switzer & Jones, 2008; Tuttle et al., 2004; Watanabe et al., 2017, 2018). Nevertheless, recent observations of apparent infragravity (IG) dominated flooding during storm and swell events appear very *tsunami-like* due to the generated *extreme* runup (Roeber & Bricker, 2015). Recently, Dewey and Ryan (2017) discovered that the boulderite deposits in the northwest of Ireland were created by storm waves and not a tsunami. In the winter of 2013–2014 storms transported boulders, weighing more than 45 metric ton, to inland distances of 222 m (Cox et al., 2018; Kennedy et al., 2017). Also, storm surge from typhoon Haiyan deposited boulders on the reef flat and a sand sheet reaching about 300 m inland (Soria et al., 2018). These observations indicate that there is a possibility for some of the relict deposits cited above to be attributed to wind wave events. The differences in overland flow dynamics between tsunamis and energetic IG waves have not been studied, hence increasing the difficulty when distinguishing between the two events from an overland flow perspective. Also, the mechanism of large IG runup is poorly understood making it difficult to determine when/where IG events could be generated. Two primary considerations in areas that are prone to both large IG and large tsunami events are as follows: (1) how do the onshore hazards themselves compare and (2) can the IG and tsunami deposits be distinguished from one another?

Long waves, such as IG waves, tend to go unnoticed to human perception. Therefore, for many years there was little knowledge of IG waves since no research was conducted to study such events. In the mid-1900's Munk and Tucker made groundbreaking discoveries about IG waves (Munk, 1949; Tucker, 1950). IG waves (60–300 s) are waves with higher periods than surface gravity waves (2–20 s) but lower periods than tsunamis (600–6,000 s). IG waves are generated through nonlinear interactions and unsteady wave setup (Biesel, 1952; Gallagher, 1971; Phillips, 1960; Young & Eldeberky, 1998). Large wind wave runup events are influenced by IG waves, local resonance of IG waves, three-wave interactions, bore-bore capture, and the local beach profile (García-Medina et al., 2017; Roeber & Bricker, 2015; Sheremet et al., 2014; Shimozono et al., 2015).

Generation mechanisms for tsunamis have been studied for decades and are well understood (Kanamori, 1972). Tsunamis can be triggered by earthquakes (Okal & Borrero, 2011), landslides (Fritz et al., 2009), volcanic eruptions (McCoy & Heiken, 2000), or meteor impacts (Weiss et al., 2015). By analyzing the wave height, flow dynamics, runup, and flooding characteristics of a tsunami, sediment deposits can be assigned to a tsunami event given their sedimentary patterns and characteristics (Chagué-Goff et al., 2011, 2015; Goff et al., 2012; Szczuciński et al., 2012). Overland flow behavior of tsunamis has been studied (Kriebel et al., 2017; Lynett, 2016; Lynett et al., 2017; Montoya et al., 2017; Park et al., 2013), but little research has been done comparing the overland flow dynamics of both tsunamis and energetic IG wave events.

Tsunamis and energetic IG waves pose a hazard to coastal communities. Both phenomena can be associated with loss of lives, injuries, and coastal damage. Accurate deposit characterization is essential to the development of reliable local databases of past flooding events. In this study we analyze the differences in overland flow behavior of tsunamis and energetic IG waves using a state of the art Boussinesq numerical model. By better understanding the differences in flow behavior between tsunamis and energetic IG waves, more accurate sedimentological studies and deposit characterization can be developed by geologists.

2. Methods

2.1. Field Observations

On 8 November 2013 Typhoon Haiyan generated large surge and waves and devastated, among many others, the coastal town of Hernani in the Philippines (Nobuoka et al., 2014). Typhoon Haiyan killed more than 6,300 people and injured more than 28,689 in the Philippines (Lagmay et al., 2014). In Hernani, deposits of sand were found ~300 m inland after the storm (Soria et al., 2018). Since Hernani is protected by an extensive fringing reef, a hazard reduction from the storm was expected (Ferrario et al., 2014). During the typhoon, several extreme IG waves or tsunami-like waves were generated and struck the coastal town (Roeber & Bricker, 2015). Video recording of one of the extreme IG waves shows that in a matter of seconds a house, located about 3 m above mean sea level (Roeber & Bricker, 2015), is washed away. This documented event has been very useful in the study of these types of phenomena and is used in the present study to test the hypothesis postulated.

Another IG event took place near Half Moon Bay, California, USA, during a surf competition on 13 February 2010. Spectators were enjoying a sunny day when suddenly an extreme IG wave washed away several people causing injuries to 13 of them (The Times, 2011). In Oregon's past storm seasons, more than 21 people have died since 1990 due to *sneaker* (IG) waves (The Oregonian, 2016). Recently several people have died in Cabo San Lucas, Mexico, when they were dragged out to sea by an extreme IG wave during a sunny day walking at the beach (Chicago Tribune, 2017). From these events it has become clear that extreme IG waves often occur during stormy conditions, but not always.

2.2. Tsunami and IG Modeling

The Cornell University Long Wave (COULWAVE) model is used in this study because of its capabilities in predicting the dynamics and formation of IG waves and runup. COULWAVE is a Boussinesq-based numerical model (Kim et al., 2009; Lynett & Liu, 2002) able to simulate wave propagation from deep water ($\frac{\text{wavelength}}{\text{depth}} \geq 2$) to the shoreline with high accuracy (Wei et al., 1995). COULWAVE has been validated, and it has been used for a wide range of applications such as wave runup, propagation, inundation, wave breaking, tsunamis, currents in ports and harbors, and hurricane waves (Lovolt et al., 2013; Lynett, 2007; Lynett et al., 2014; Parsons et al., 2014, among others). This model solves the fully nonlinearly, weakly dispersive wave equations given in the one-dimensional conservative form as

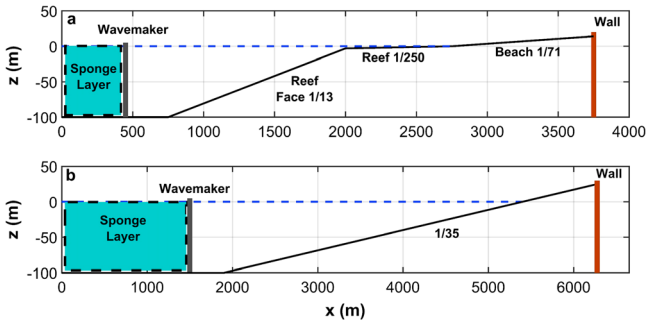

Figure 1. Transects used for Cornell University Long Wave (COULWAVE) tsunami and infragravity simulations, (a) Reef case and (b) planar beach case. A sponge layer and a wall are used at the left and right boundary, respectively. A 1/250 reef profile is used to represent a generic, shelf/reef coastal profile. This is a very mild reef slope and effectively flat for the incoming waves.

$$H_t + (U_\infty H)_x + D^c = 0 \quad (1)$$

$$(U_\infty H)_t + \left(U_\infty^2 H\right)_x + gH\zeta_x + gHD^x - U_\infty D^c = 0 \quad (2)$$

where $H = \zeta + h$ is the total water depth, U_∞ denotes the velocity at a reference elevation z_∞, D^x is the second-order terms of the depth-integrated momentum equation and averaged velocities, and D^c includes the second-order terms of the continuity equation. A spatially constant bottom friction of $f = 0.0035$ was used with a quadratic bottom friction law for the model simulations.

A fully nonlinear Boussinesq model is used for several reasons. As the waves propagate onto the surf zone and reef, they undergo important transformations due to nonlinear shoaling, reflection, breaking, and wave-wave interactions. The surf zone is an area with strong nonlinearities, and the wave height to water depth ratios during these processes can be unsuitable for weakly nonlinear Boussinesq models (Shi et al., 2012; Wei et al., 1995). For more reliable model estimates (wave height, runup, etc.) high-order interactions should be incorporated due to the strong nonlinearities found in the surf zone (de Bakker et al., 2015; Nwogu, 1993; Thomson et al., 2006).

For the generation of energetic IG waves an internal-domain wave-maker is used in COULWAVE, driven by a Joint North Sea Wave Project (JONSWAP) input spectrum. A JONSWAP spectrum is used as it is capable of representing tropical cyclone waves (Hwang et al., 2017; Ochi & Chiu, 1982; Young, 2017). A wall is located at the right boundary and a sponge layer at the left boundary. A grid resolution of 2 m is used for all the simulations. The tsunamis are modeled as a single symmetric amplitude dipole. A grid resolution of 20 m is used for all tsunami simulations. The rest of the parameters from COULWAVE were kept the same as in the IG wave simulations.

For the IG simulations, the incident shortwave condition is discretized with a very small frequency resolution (10^{-4} Hz). Different configurations of significant wave heights (H_s = 3 to 12 m) and peak periods (T_p = 13 to 22 s) were tested (total of 100 configurations). Each configuration was simulated 10 times and had a unique random phase seed yielding a different deterministic representation of the input wave energy spectrum. After simulating more than a million waves, only five extreme IG runup events were detected (generated when $H_s > 11$ m and $T_P > 20$ s). An extreme or very rare IG runup is defined here as a runup elevation that is 5 standard deviations above the mean or a 5-sigma event. The combination of waves with $H_s > 11$ m and $T_p > 20$ s is not very common but has been observed in tropical cyclones (Bowyer & MacAfee, 2005; MacAfee & Bowyer, 2005), big swell events, and storm events in northwest Europe (Gallagher et al., 2016; Masselink et al., 2016).

Two different profiles (planar beach and reef case) are used to study the overland flow dynamics of both tsunamis and IG waves (Figure 1). As was previously mentioned, tsunamis are modeled as a single symmetric amplitude dipole with both a leading and following depression. The period of the tsunamis tested in this study, defined as two times the duration between the peak of the crest and minimum of the trough, range from 6 to 22 min. To make a valid comparison between the tsunami and extreme IG event, two different control criteria were used: maximum runup elevation and maximum offshore crest elevation. For the first criterion, where the maximum runup elevation for both the tsunami and IG are equal, different offshore tsunami amplitudes had to be tested until we found a tsunami with the same runup as the extreme IG event. Alternatively, when matching maximum offshore crest elevation, tsunami simulations were initialized with an offshore (at 100-m depth) crest elevation equal to the offshore wind wave amplitude that produced the extreme runup in the IG simulation.

3. Results and Discussion

Figure 2a shows the 100-m depth ocean surface elevation time series (x = 750 m) for the IG reef case simulation. Only one out of the five extreme events is used in this analysis as all have similar runup elevations and overland flow behavior. The wave parameters for the input spectrum that generated this extreme are H_s = 11 m and T_p = 21 s. The maximum runup elevation generated for the reef bathymetry is 8.05 m with

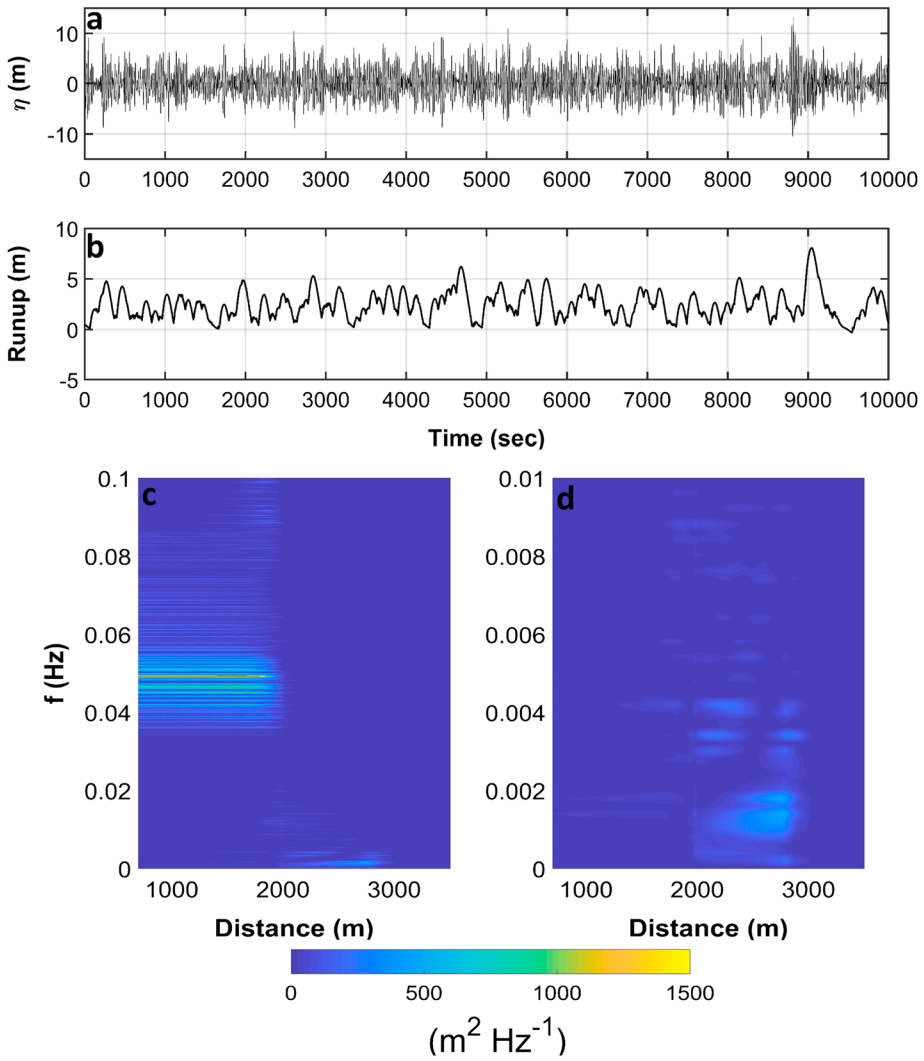

Figure 2. (a) Offshore (x = 750 m) free surface elevations and (b) runup time series for the infragravity (IG) configuration that generated an extreme runup event (reef case). A maximum runup elevation of 8.05 m and a dominant runup period of about 650 s were predicted by Cornell University Long Wave (COULWAVE). Frequency spectrum of water surface elevation along the one-dimensional reef transect from COULWAVE IG simulations (reef case): (c) Plot for a broad frequency range and (d) zoomed in on IG frequencies.

a dominant runup period of about 650 s (Figure 2b). Dominant runup period is defined in this study as the approximate time in between runup peaks. A spectrum of low-frequency runup height oscillations can also be observed in Figure 2b. The maximum wave crest height of the incident wave train that generated the maximum runup is 11.37 m. For the planar beach case, a slope of 1/35 is used since it represents the average slope of the entire reef configuration. For the planar beach, the maximum runup is 11.76 m and a dominant runup period of about 200 s (not shown). To match the maximum tsunami runup elevation with the IG event runup, offshore tsunami crest heights (at 100-m depth) ranging from 4.2 to 5 and from 3.2 to 4 m are used for the reef configuration and the planar beach, accordingly. The tsunami height changes depending on the tsunami period and whether there is a leading or following trough.

Figure 2c presents a frequency spectrum across the reef for the IG wind wave simulation. It shows that the offshore incident waves break just before the reef at x = 2,000 m. A preliminary analysis of the generation mechanisms of large IG runup shows that two or more sets/envelopes of highly nonlinear waves, with particular characteristics (envelope duration, mean crest height, Ursell number, etc …), are needed to generate extreme runup events. The IG energy arises through nonlinear interactions within the wave spectrum; it is released as free wave energy as the wave breaks, and the reef/beach is selectively excited with IG energy

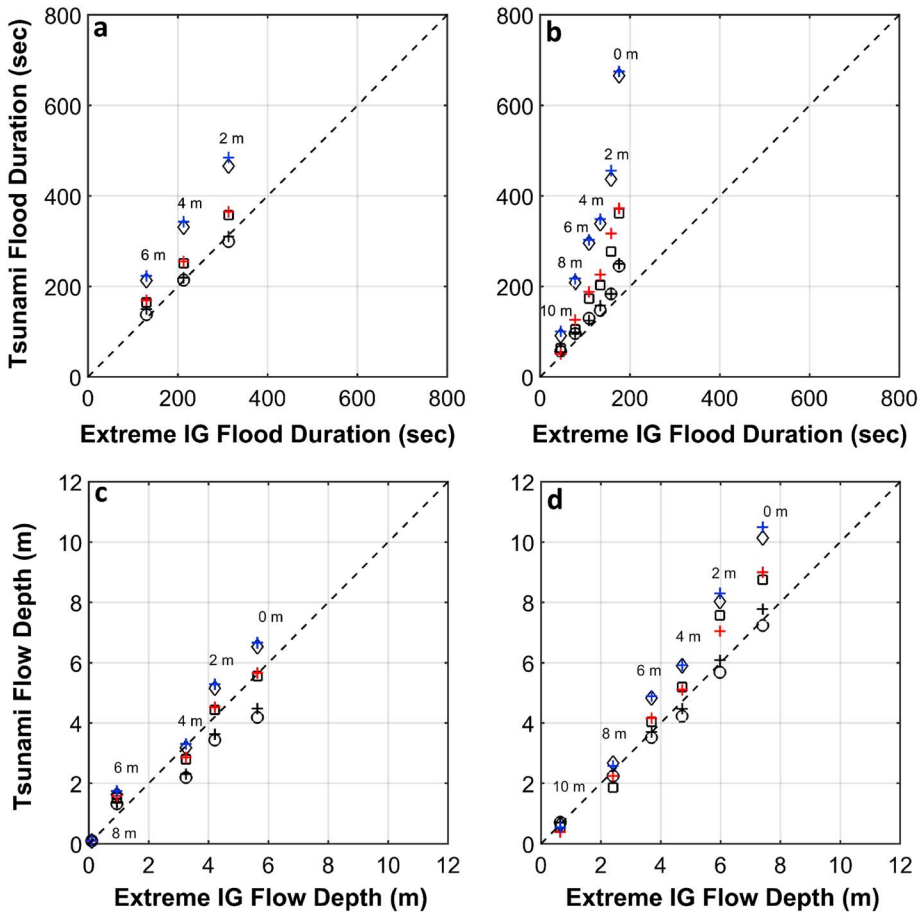

Figure 3. Comparison of flood duration and flow depths between infragravity (IG) and tsunami for the (a and c) reef case and (b and d) planar beach case. Leading crest and leading depression tsunami predictions, for a period of 6 min, are presented with a circle and a black cross, respectively. Tsunami period of 11 min are presented with a square (leading crest) and a red cross (leading depression). Tsunami period of 22 min are presented with a diamond (leading crest) and a blue cross (leading depression).

at the resonant modes (Figure 2d). If the bathymetry is modified, it would change the nonlinear transfers, the breakpoint, and the resonant modes, having a strong effect on which incident wave sets might lead to very large runup events. This topic requires further investigation beyond the scope of this paper.

To better understand the overland flow dynamics between tsunamis and IG waves, this study presents comparisons of flood duration, flow depth, maximum overland flow velocity, and Froude number (Fr). Maximum velocities are calculated using a 0.3-m depth threshold in order to reduce the relevance of very thin, but fast moving flows. Measurements are compared at four different profile elevations for the reef configuration (0, 2, 4, and 6 m) and six elevations for the planar beach configuration (0, 2, 4, 6, 8, and 10 m). Figure 3a shows that for the reef configuration, the ground was usually flooded longer during the tsunami event for the tsunami periods tested, as compared to the IG event flood duration. However, flood durations are very similar for both mechanisms when the tsunami has a period of 6 min. For the planar beach, Figure 3b shows that flood duration is greater for tsunami waves than IG for all tsunami periods. Also, comparable to the reef, both events tend to yield similar flood durations for small tsunami periods ($<$6 min). There is little difference in the results when there is a leading depression first in the tsunami. Overall, tsunamis tend to flood the entire profile for a longer time in both model configurations.

For the reef, Figure 3c shows that tsunami and energetic IG flow depths are very similar for tsunami periods comparable to the IG dominant runup period (~11 min). When the tsunami period is greater than the IG dominant period, the tsunami flow depths tend to be larger. Also, tsunami flow depths are found to be greater than IG flow depths at the upper beach (6-m elevation) for all tsunami periods. Figure 3d shows

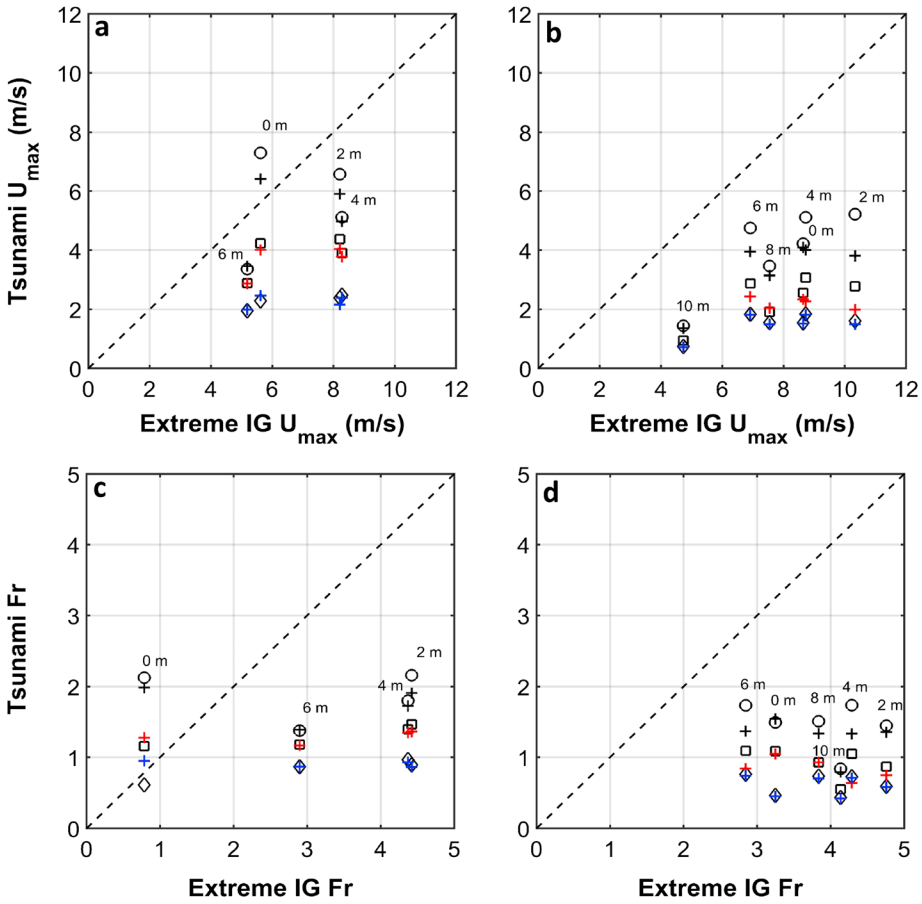

Figure 4. Comparison of flow speeds and Froude number between infragravity (IG) and tsunami for the (a and c) reef case and planar (b and d) beach case. Leading crest and leading depression tsunami predictions, for a period of 6 min, are presented with a circle and a black cross, respectively. Tsunami period of 11 min are presented with a square (leading crest) and a red cross (leading trough). Tsunami period of 22 min are presented with a diamond (leading crest) and a blue cross (leading trough).

that for the planar beach, tsunami flow depths are usually greater than IG flow depths. When the tsunami period is 6 min, flow depths from both events are almost the same. Generally, tsunamis tend to have a greater flow depth throughout the entire profile in both configurations; however, when the IG dominant runup period and tsunami period are similar, their flow depths are similar.

Figure 4a shows that for the reef, IG maximum flow speeds are higher than tsunami flow speeds throughout the beach profile, except at the shoreline when tsunami period is 6 min. A similar behavior is observed for the Fr (Figure 4c). Away from the immediate shoreline, the maximum Fr is always greater for the energetic IG event. Finally, for the planar beach, IG flow velocities and Fr were much larger than tsunami flow speeds as shown in Figures 4b and 4d. Regardless of the tsunami period, the Fr for IG is always higher, and for some locations approaches a value of 5. As the waves travel to the beach they have a Fr of less than 1, but as they begin to break near the beach the Fr gets close to 1 and in some instances greater than 1 after breaking. In order for the Fr to be greater than 1 after the waves break there has to be an increase in the flow at low depths. This happens with bore-bore capture, that is, as a bore collapses on the beach the transferred momentum increases the velocities at low depths (García-Medina et al., 2017). Therefore, bore renewal with bore-bore capture contributes to these larger flow speeds and increases the Fr. Energetic IG shows greater speeds and Fr with smaller depths in both configurations tested.

To further investigate the overland flow behavior of these two flooding mechanism, a second control criterion is used in which the same maximum offshore wave crest height from the IG simulations is used for the tsunami simulations. An offshore wave crest height of 11.37 m for the tsunami is adopted, as previously

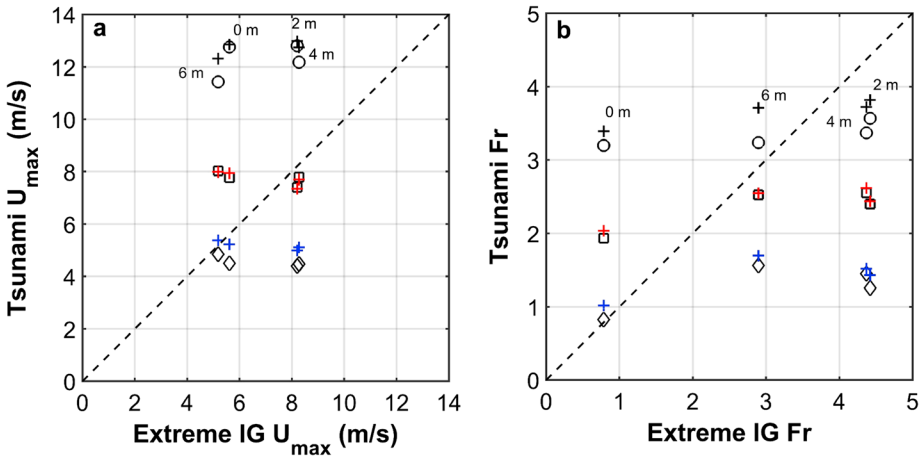

Figure 5. Comparison of (a) flow speeds and (b) Fr between infragravity (IG) and tsunami for the reef. Leading crest and leading depression tsunami predictions, for a period of 6 min, are presented with a circle and a black cross, respectively. Tsunami period of 11 min are presented with a square (leading crest) and a red cross (leading trough). Tsunami period of 22 min are presented with a diamond (leading crest) and a blue cross (leading trough).

mentioned. It is important to note that the tsunami runup is much larger than the IG runup (~20 m versus ~9 m). For this comparison, only results from the reef are presented as very similar results are obtained for the planar beach. Figure 5a shows that for tsunami periods less than the dominant runup period, tsunami velocities are larger than IG velocities. As tsunami period increases, the velocities decrease throughout the beach profile. Fr is greater across the profile for the tsunamis, except at 2- to 4-m elevation, when the tsunami period is less than the IG runup dominant period as shown in Figure 5b. When the tsunami period increases, Fr is greater for IG everywhere along the profile except at the shoreline. It is worthwhile to reiterate that for this offshore-amplitude-match scenario, where the maximum tsunami runup elevation is much greater than the IG runup, there are still locations along the beach profile where the extreme IG flooding leads to larger maximum fluid speeds and larger maximum Froude numbers.

4. Conclusions

Extreme IG-driven runup events can appear tsunami-like and, for the wave conditions prescribed herein, can lead to runup elevations in excess of 10 m above storm water level. In general, whenever the tsunamis and energetic IG waves have similar runup it is determined that tsunami flow depths and flood durations are greater. On the other hand, the maximum IG flow speeds are greater in most of the cases, particularly when tsunamis have a long period (>6 min). Also, IG maximum Fr is greater than the tsunami maximum Fr in the majority of cases. For the IG simulations, the large Fr appears to be generated by bore-bore capture. Furthermore, when tsunami runup is much larger than IG runup (with matching maximum incident offshore crest heights) the IG speeds can be greater when tsunami periods are greater than the dominant IG period. Tsunamis and energetic IG of similar amplitude/period lead to differences in flow properties, and it is consequently expected that these differences influence the resulting sedimentology.

There are several challenges that exist in order to discriminate tsunami events from extreme IG events. First is the lack of identified extreme IG deposits. Furthermore, for coastal areas that are prone to both large tsunamis and large wind wave events, the local statistics of extreme IG/wind wave runup needs to be analyzed and understood. The periods at which the local beach excite or trap IG energy needs to be investigated since the longer the IG period, the further onshore the water can travel. Also, the return periods of tsunamis and large wind wave runup need to be compared at hazard levels of interest. Areas where the return periods are not comparable could be used to identify where deposits, boulders, and design hazards can be more reliably attributed.

Acknowledgments
Primary support for this work has been provided by the National Science Foundation grant 1538624 and 1661052. All supplemental data can be accessed from https://github.com/Luigi2015/tsunami_IG. Special thanks to Adam Keen and William Dally for the insightful comments. Finally, thanks for the comments made by the anonymous reviewers, which led to significant improvements to this manuscript.

References

de Bakker, A. T., Herbers, T. H., Ruessink, B. G., Smit, P. B., & Tissier, M. F. (2015). Nonlinear Infragravity–wave interactions on a gently sloping laboratory beach. *Journal of Physical Oceanography*, *45*(2), 589–605. https://doi.org/10.1175/JPO-D-14-0186.1

Biesel, F. (1952). Equations generales au second ordre de la houle irreguliere. *La Houille Blanche*, *5*, 372–376.

Bowyer, P. J., & MacAfee, A. W. (2005). The theory of trapped-fetch waves with tropical cyclones—An operational perspective. *Weather Forecasting*, *20*(3), 229–244. https://doi.org/10.1175/WAF849.1

Chagué-Goff, C., Goff, J., Wong, H. K. Y., & Cisternas, M. (2015). Insights from geochemistry and diatoms to characterise a tsunami's deposit and maximum inundation limit. *Marine Geology*, *359*, 22–34. https://doi.org/10.1016/j.margeo.2014.11.009

Chagué-Goff, C., Schneider, J.-L., Goff, J. R., Dominey-Howes, D., & Strotz, L. (2011). Expanding the proxy toolkit to help identify past events—Lessons from the 2004 Indian Ocean tsunami and the 2009 South Pacific tsunami. *Earth-Science Reviews*, *107*(1-2), 107–122. https://doi.org/10.1016/j.earscirev.2011.03.007

Chicago Tribune (2017). Retrieved from http://www.chicagotribune.com/, last access: 4 April 2018.

Cox, R., Jahn, K. L., Watkins, O. G., & Cox, P. (2018). Extraordinary boulder transport by storm waves (west of Ireland, winter 2013–2014) and criteria for analyzing coastal boulder deposits. *Earth-Science Reviews*, *177*, 623–636. https://doi.org/10.1016/j.earscirev.2017.12.014

Dewey, J. F., & Ryan, P. D. (2017). Storm, rogue wave, or tsunami origin for megaclast deposits in western Ireland and North Island, New Zealand? *Proceedings of the National Academy of Sciences*, *114*(50), E10639–E10647. https://doi.org/10.1073/pnas.1713233114

Ferrario, F., Beck, M. W., Storlazzi, C. D., Micheli, F., Shepard, C. C., & Airoldi, L. (2014). The effectiveness of coral reefs for coastal hazard risk reduction and adaptation. *Nature Communications*, *5*(1), 3794. https://doi.org/10.1038/ncomms4794

Fritz, H. M., Mohammed, F., & Yoo, J. (2009). Lituya Bay landslide impact generated mega-tsunami 50th anniversary. *Pure and Applied Geophysics*, *166*(1-2), 153–175. https://doi.org/10.1007/s00024-008-0435-4

Gallagher, B. (1971). Generation of surf beat by nonlinear wave interactions. *Journal of Fluid Mechanics*, *49*(01), 1–20. https://doi.org/10.1017/S0022112071001897

Gallagher, S., Gleeson, E., Tiron, R., McGrath, R., & Dias, F. (2016). The nearshore wind and wave energy potential of Ireland: A high resolution assessment of availability and accessibility. *Renewable Energy*, *88*, 494–516. https://doi.org/10.1016/j.renene.2015.11.010

García-Medina, G., Özkan-Haller, H. T., Holman, R. A., & Ruggiero, P. (2017). Large runup controls on a gently sloping dissipative beach. *Journal of Geophysical Research: Oceans*, *122*, 5998–6010. https://doi.org/10.1002/2017JC012862

Goff, J., Chagué-Goff, C., Nichol, S., Jaffe, B., & Dominey-Howes, D. (2012). Progress in palaeotsunami research. *Sedimentary Geology*, *243–244*, 70–88.

Hwang, P. A., Fan, Y., Ocampo-Torres, F. J., & García-Nava, H. (2017). Ocean surface wave spectra inside tropical cyclones. *Journal of Physical Oceanography*, *47*(10), 2393–2417. https://doi.org/10.1175/JPO-D-17-0066.1

Kanamori, H. (1972). Mechanism of tsunami earthquakes. *Physics of the Earth and Planetary Interiors*, *6*, 346–359.

Kennedy, A. B., Mori, N., Yasuda, T., Shimozono, T., Tomiczec, T., Donahue, A., et al. (2017). Extreme block and boulder transport along a cliffed coastline (Calicoan Island, Philippines) during Super Typhoon Haiyan. *Marine Geology*, *383*, 65–77.

Kim, D. H., Lynett, P. J., & Socolofsky, S. A. (2009). A depth-integrated model for weakly dispersive, turbulent, and rotational fluid flows. *Ocean Modelling*, *27*(3-4), 198–214. https://doi.org/10.1016/j.ocemod.2009.01.005

Kriebel, D., Lynett, P., & Cox, D. (2017). Energy method for approximating overland tsunami flows. *Journal of Waterway, Port, Coastal, and Ocean Engineering (ASCE)*, *143*(5), 04017014. https://doi.org/10.1061/(asce)ww.1943-5460.0000393

Lagmay, A. M., Agaton, R. P., Bahala, M. A. C., Briones, J. B. L. T., Cabacaba, K. M. C., & Caro, C. V. C. (2014). Devastating storm surges of Typhoon Haiyan. *International Journal of Disaster Risk Reduction*, *11*, 1–12. https://doi.org/10.1016/j.ijdrr.2014.10.006

Lovolt, F., Pedersen, G., & Lynett, P. (2013). Simulating run-up on steep slopes with operational Boussinesq models; capabilities, spurious effects and instabilities. *Natural Hazards and Earth System Sciences*, *20*(3), 379–395. https://doi.org/10.5194/npg-20-379-2013

Lynett, P. (2007). The effect of a shallow water obstruction on long wave runup and overland flow velocity. *Journal of Waterway, Port, Coastal, and Ocean Engineering (ASCE)*, *133*(6), 455–462. https://doi.org/10.1061/(ASCE)0733-950X(2007)133:6(455)

Lynett, P. (2016). Precise prediction of coastal and overland flow dynamics: A grand challenge or a fool's errands. *Journal of Disaster Research*, *11*(4), 615–623. https://doi.org/10.20965/jdr.2016.p0615

Lynett, P., Borrero, J., Son, S., Wilson, R., & Miller, K. (2014). Assessment of the tsunami-induced current hazard. *Geophysical Research Letters*, *41*, 2048–2055. https://doi.org/10.1002/2013GL058680

Lynett, P. J., & Liu, P. L.-F. (2002). A two-dimensional, depth-integrated model for internal wave propagation over variable bathymetry. *Wave Motion*, *36*(3), 221–240. https://doi.org/10.1016/S0165-2125(01)00115-9

Lynett, P. J., Gately, K., Wilson, R., Montoya, L., Arcas, D., Aytore, B., et al. (2017). Inter-model analysis of tsunami induced currents. *Ocean Model*, *114*, 14–32. https://doi.org/10.1016/j.ocemod.2017.04.003

MacAfee, A. . W., & Bowyer, P. (2005). The modeling of trapped-fetch waves with tropical cyclones—A desktop operational model. *Weather Forecasting*, *20*(3), 245–263. https://doi.org/10.1175/WAF850.1

Mamo, B., Strotz, L., & Dominey-Howes, D. (2009). Tsunami sediments and their foraminiferal assemblages. *Earth-Science Reviews*, *96*(4), 263–278. https://doi.org/10.1016/j.earscirev.2009.06.007

Masselink, G., Castelle, B., Scott, T., Dodet, G., Suanez, S., Jackson, D., & Floc'h, F. (2016). Extreme wave activity during2013/2014 winter and morphological impacts along the Atlantic coast of Europe. *Geophysical Research Letters*, *43*, 2135–2143. https://doi.org/10.1002/2015GL067492

McCoy, F. W., & Heiken, G. (2000). Tsunami generated by the Late Bronze Age eruption of Thera (Santorini), Greece. *Pure and Applied Geophysics*, *157*(6-8), 1227–1256. https://doi.org/10.1007/s000240050024

Montoya, L., Lynett, P., Thio, H., & Li, W. (2017). Spatial statistics of tsunami overland flow properties. *Journal of Waterway, Port, Coastal, and Ocean Engineering (ASCE)*, *143*(2). https://doi.org/10.1061/(ASCE)WW.1943-5460.0000363

Morton, R. A., Gelfenbaum, G., & Jaffe, B. E. (2007). Physical criteria for distinguishing sandy tsunami and storm deposits using modern examples. *Sedimentary Geology*, *200*(3-4), 184–207. https://doi.org/10.1016/j.sedgeo.2007.01.003

Munk, W. H. (1949). Surf beats. *Eos, Transactions American Geophysical Union*, *30*, 849–854.

Nobuoka, H., Yasuda, T., Tajima, Y., Mori, N., Shimozono, T., Sasaki, J., et al. (2014). Coastal flood disaster due to historic Typhoon Haiyan in Hernani, Eastern Samar Province, Philippines. J. Jpn Soc. Civil Eng. Ser. B2 70, I_1426–I_1430 in Japanese.

Nwogu, O. (1993). Alternative form of Boussinesq equations for nearshore wave propagation. *Journal of Waterway, Port, Coastal, and Ocean Engineering (ASCE)*, *119*(6), 618–638. https://doi.org/10.1061/(ASCE)0733-950X(1993)119:6(618)

Ochi, M. K., & Chiu, M. H. (1982). Nearshore wave spectra measured during Hurricane David. 18th International Conference on Coastal Engineering (pp. 77–86). Cape Town.

Okal, E. A., & Borrero, J. C. (2011). The "tsunami earthquake" of 22 June 1932 in Manzanillo, Mexico: Seismological study and tsunami simulations. *Geophysical Journal International*, *187*(3), 1443–1459. https://doi.org/10.1111/j.1365-246X.2011.05199.x

Park, H., Cox, D., Lynett, P., Wiebe, D., & Shin, S. (2013). Tsunami inundation modeling in constructed environments: A physical and numerical comparison of free-surface elevation, velocity, and momentum flux. *Coastal Engineering*, *79*, 9–21. https://doi.org/10.1016/j.coastaleng.2013.04.002

Parsons, T., Geist, E., Ryan, H., Lee, H., Haeussler, P., Lynett, P., et al. (2014). Source and progression of a submarine landslide and tsunami: The 1964 Great Alaska earthquake at Port Valdez. *Journal of Geophysical Research: Solid Earth*, *119*, 8502–8516. https://doi.org/10.1002/2014JB011514

Phantuwongraj, S., & Choowong, M. (2012). Tsunamis versus storm deposits from Thailand. *Natural Hazards*, *63*(1), 31–50. https://doi.org/10.1007/s11069-011-9717-8

Phillips, O. M. (1960). On the dynamics of unsteady gravity waves of finite amplitude. Part 1. The elementary interactions. *Journal of Fluid Mechanics*, *9*(2), 193–217. https://doi.org/10.1017/S0022112060001043

Roeber, V., & Bricker, J. D. (2015). Destructive tsunami-like wave generated by surf beat over a coral reef during Typhoon Haiyan. *Nature Communications*, *6*(1), 7854. https://doi.org/10.1038/ncomms8854

Sheremet, A., Staples, T., Ardhuin, F., Suanez, S., & Fichaut, B. (2014). Observations of large infragravity wave runup at Banneg Island, France. *Geophysical Research Letters*, *41*, 976–982. https://doi.org/10.1002/2013GL058880

Shi, F., Kirby, J. T., Geiman, J. D., & Grilli, S. (2012). A high-order adaptive time-stepping TVD solver for Boussinesq modeling of breaking waves and coastal inundation. *Ocean Modelling*, *43*, 36–51.

Shimozono, T., Tajima, Y., Kennedy, A. B., Nobuoka, H., Sasaki, J., & Sato, S. (2015). Combined infragravity wave and sea-swell runup over fringing reefs by super typhoon Haiyan. *Journal of Geophysical Research: Oceans*, *120*, 4463–4486. https://doi.org/10.1002/2015JC010760

Soria, J. L. A., Switzer, A. D., Pilarczyk, J. E., Tang, H., Weiss, R., Siringan, F., et al. (2018). Surf beat-induced overwash during Typhoon Haiyan deposited two distinct sediment assemblages on the carbonate coast of Hernani, Samar, central Philippines. *Marine Geology*, *396*, 215–230. https://doi.org/10.1016/j.margeo.2017.08.016

Switzer, A. D., & Jones, B. G. (2008). Setup, deposition and sedimentary characteristics of two storm overwash deposits, Abrahams Bosom Beach, southeastern Australia. *Journal of Coastal Research*, *24*, 189–200.

Szczuciński, W., Kokociński, M., Rzeszewski, M., Chagué-Goff, C., Cacho, M., Goto, K., & Sugawara, D. (2012). Sediment sources and sedimentation processes of 2011 Tohoku-oki tsunami deposits on the Sendai Plain, Japan—Insights from diatoms, nannoliths and grain size distribution. *Sedimentary Geology*, *282*, 40–56. https://doi.org/10.1016/j.sedgeo.2012.07.019

The Oregonian (2016). Retrieved from http://www.oregonlive.com/, last access: 4 April 2018.

The Times (2011). Retrieved from http://www.thetimes.com/, last access: 4 April 2018.

Thomson, J., Elgar, S., Raubenheimer, B., Herbers, T. H. C., & Guza, R. T. (2006). Tidal modulation of infragravity waves via nonlinear energy losses in the surfzone. *Geophysical Research Letters*, *33*, L05601. https://doi.org/10.1029/2005GL025514

Tucker, M. J. (1950). Surf beats: Sea waves of 1–5 minute period. *Proceedings of the Royal Society of London. Series A: Mathematical and Physical Sciences*, *202*(1071), 565–573. https://doi.org/10.1098/rspa.1950.0120

Tuttle, M. P., Ruffman, A., Anderson, T., & Jeter, H. (2004). Distinguishing tsunami from storm deposits in eastern North America: The 1929 Grand Banks Tsunami versus the 1991 Halloween Storm. *Seismological Research Letters*, *75*(1), 117–131. https://doi.org/10.1785/gssrl.75.1.117

Watanabe, M., Bricker, J. D., Goto, K., & Imamura, F. (2017). Factors responsible for the limited inland extent of sand deposits on Leyte Island during 2013 Typhoon Haiyan. *Journal of Geophysical Research: Oceans*, *122*, 2795–2812. https://doi.org/10.1002/2016JC012023

Watanabe, M., Goto, K., Bricker, J. D., & Imamura, F. (2018). Are inundation limit and maximum extent of sand useful for differentiating tsunamis and storms? An example from sediment transport simulations on the Sendai Plain, Japan. *Sedimentary Geology*, *364*, 204–216. https://doi.org/10.1016/j.sedgeo.2017.12.026

Wei, G., Kirby, J. T., Grilli, S. T., & Subramanya, R. (1995). A fully nonlinear Boussinesq model for surface waves: Part I. Highly nonlinear unsteady waves. *Journal of Fluid Mechanics*, *294*(1), 71–92. https://doi.org/10.1017/S0022112095002813

Weiss, R., Lynett, P., & Wünnemann, K. (2015). The Eltanin impact and its tsunami along the coast of South America: Insights for potential deposits. *Earth and Planetary Science Letters*, *409*, 175–181. https://doi.org/10.1016/j.epsl.2014.10.050

Young, I. R. (2017). A review of parametric descriptions of tropical cyclone wind-wave generation. *Atmosphere*, *8*(12), 194. https://doi.org/10.3390/atmos8100194

Young, I. R., & Eldeberky, Y. (1998). Observations of triad coupling of finite depth wind-waves. *Coastal Engineering*, *33*(2-3), 137–154. https://doi.org/10.1016/S0378-3839(98)00006-4

Erratum

In the originally published version of this article, there was an error in the fourth paragraph of section 2.2, "Tsunami and IG Modeling." The first sentence of this paragraph, "For the IG simulations, the incident shortwave condition is discretized with a very small frequency resolution (10^{-5} Hz)," should have read "For the IG simulations, the incident shortwave condition is discretized with a very small frequency resolution (10^{-4} Hz)." This error has since been corrected, and this version may be considered the authoritative version of record